Experimental Study of Compton Scattering Reduction in Digital Mammographic Imaging

S. R. Amendolia, M. G. Bisogni, P. Delogu, M. E. Fantacci, M. Novelli, P. Oliva, M. Quattrocchi, V. Rosso, A. Stefanini, and Sergio Zucca

***Abstract*—In mammography, the first cause of image contrast reduction arises from the photons scattered inside the examined organ. The amount of Compton scattering strongly depends on the irradiation area and on the distance between the organ and the X-ray detector. We have experimentally evaluated how these geometrical conditions affect the scattering fraction. Our experimental setup includes a single photon counting device based on a silicon pixel detector as X-ray sensor, a lucite cylinder to simulate the breast tissue, and a lead collimator to define the irradiation area. We have evaluated the contrast and the signal-to-noise ratio for images acquired in different conditions.**

***Index Terms*—Contrast, mammography, pixel detector, scattered photons, signal-to-noise ratio (SNR), single photon counting chip.**

I. Introduction

THE DETECTION of low-contrast structures in breast tissue represents a challenging task for mammography [1]: for tumoral masses in early development stage, the radiological contrast is below 3%.

The principal cause of contrast reduction in mammographic images is the radiation scattered by the organ [2], [3].

We know from previous Monte Carlo simulations realized by our group [4] that the scattered photons from a phantom have an average scattering angle of 0.59 rd and a full-width at half-maximum (FWHM) of 1 rd respect to the original direction. The input of the simulation is a photon beam impinging orthogonally on a 4-cm-thick lucite phantom; the photon energy distribution reproduces the one of a standard mammographic tube.

Moreover, this study shows that for an irradiation field of 18×18 cm^2, the scatter fraction (the scattered over primary flux ratio) is on the order of 70%. This implies an estimated image contrast reduction factor up to 60% with respect to the theoretical value [see (3)].

Anti-diffusion grids are used in standard mammography to reject the scattered photons; they are inserted between the patient and the radiation detector. As a drawback, they lead to a consistent increase on patient dose because part of the primary radiation is adsorbed by the grids so that, in order to have the same statistical quality, the photons flux must be increased.

Manuscript received November 8, 2001; revised May 16, 2002.

S. R. Amendolia is with the Istituto di Matematica e Fisica, Universitá of Sassari and Sezione INFN Pisa, 56010 San Piero a Grado, Pisa, Italy.

M. G. Bisogni, P. Delogu, M. E. Fantacci, M. Novelli, P. Oliva, M. Quattrocchi, V. Rosso, A. Stefanini, and S. Zucca are with the Dipartimento di Fisica dell'Universitá e Sezione INFN di Pisa, 56010 San Piero a Grado, Pisa, Italy (e-mail: sergio.zucca@pi.infn.it).

Digital Object Identifier 10.1109/TNS.2002.803816

An alternative way to reject the scatter contribution is to reduce the irradiation field by using collimator grids inserted before the patient in a projection geometry. The grids reduce the irradiation field area and are moved with a scanning technique to cover the full region of interest [5], [6]. This method allows one to reduce the scatter with no increase in the patient dose.

II. Experimental Setup

We used several 3-mm-thick lead collimators with square openings ranging from 3.61 to 56 cm^2.

The collimators were placed, in turn, above a breast phantom which consists of a lucite cylinder, 4 cm thick and 10 cm in diameter. A standard mammographic tube (0.1-mm fine focus, 1-mm Be + 0.03 mm Mo filter) was used to irradiate the phantom at a distance focus-phantom of 63 cm. A single photon counting device based on a silicon pixel detector was used as an X-ray sensor. The detector is a 300-μm thick silicon crystal with an array of 64×64 square pixels, 170 μm on each side. The data readout is performed by a photon counting chip (PCC), which is a very large scale integration (VLSI)-integrated circuit, developed as part of the MEDIPIX collaboration [7]–[9]. The electronics chip is connected to the sensor by means of bump-bonding techniques. The detector active area is 1.2 cm^2.

III. Results

A. Scattering Dependency on Irradiation Area

For every image, the number of counts/pixel, N, is the sum of two different contributions—the primary photons P that cross the phantom without change in their direction and the scattered photons S that cross the phantom interacting with the material.

If we assume that the number of primary photons per unit area is independent of position in the irradiated area, the variation of the number of counts/pixel in images with different collimators is due to the variation of the scatter contribution.

To evaluate this effect, we can write

$$\frac{S_{\text{open}} - S_x}{N_{\text{open}}} = \frac{N_{\text{open}} - N_x}{N_{\text{open}}} = 1 - \frac{N_x}{N_{\text{open}}} \tag{1}$$

$$N_{\text{open}} = P + S_{\text{open}} \qquad N_x = P + S_x \tag{2}$$

where N_{open} is the number of counts/pixel for an open irradiation field, N_x is the number of counts/pixel for an irradiation field of area x, and S_{open} and S_x are the contributions of the scattered photons for the two irradiation fields. Fig. 1 shows

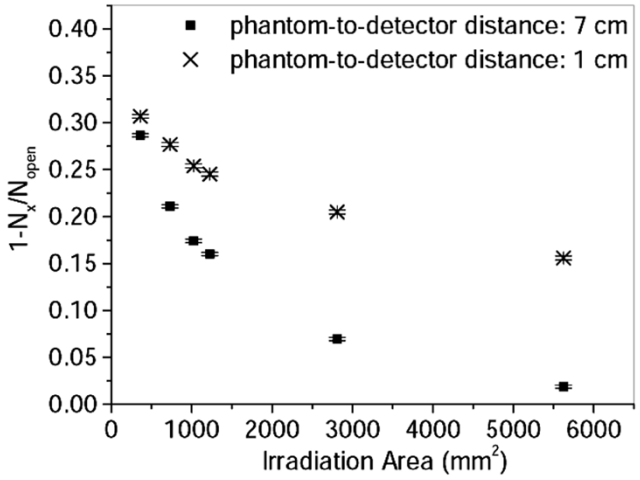

Fig. 1. Relative difference between the number of counts/pixel of the image taken with an open field $(N_{\rm open})$ and the number of counts/pixel of the image taken with a radiation field of area x (N_x). Circles represent distance phantom-detector of 1 cm, crosses represent phantom-to-detector distance of 7 cm. The error bars represent the statistical error.

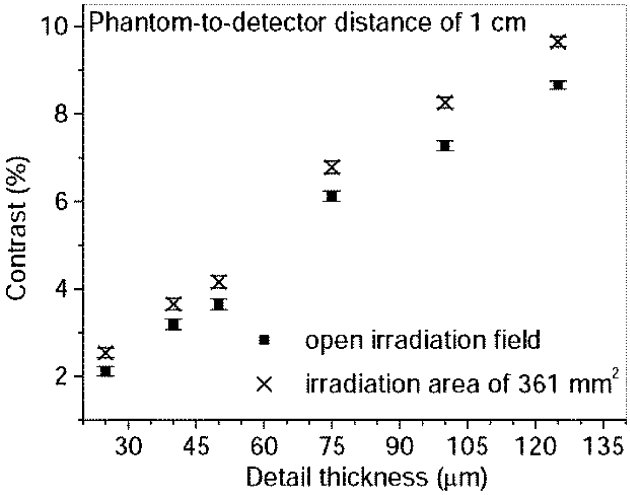

Fig. 2. Calculated contrast of aluminum details of different thickness for an open field acquisition (squares) and for an acquisition with an irradiation field area of 361 mm^2 (crosses). The error bars represent the statistic error. The distance between the phantom and the detector is 1 cm.

how the contribution of scattered photons decreases with the decrease in the irradiation field area.

B. Contrast Measurements

The reduction of the scatter photons improves the imaging capabilities and in particular the experimental contrast $C_{\rm exp}$ defined as:

$$C_{\rm exp} = \frac{C_{th}}{1 + \frac{S}{P}} \tag{3}$$

where C_{th} is the theoretical contrast related to the differences in the adsorption of photons between region of different densities within the phantom.

We have studied the improvement of the contrast at a phantom-to-detector distance of 1 cm for different irradiation areas. The phantom is a 4-cm-thick lucite cylinder in which there are various 12-mm diameter holes that are 3 mm deep.

In each hole, an aluminum detail 4 mm in diameter of different thickness, is immersed in wax. We used aluminum details with a thickness ranging from 125 μm to 25 μm. Fig. 2 shows the contrast of the aluminum details for an open field (squares) and for an irradiation field area of 361 mm^2 (crosses). The contrast improvement factor (CIF) $= C_{\rm collimated}/C_{\rm open}$ is plotted in Fig. 3. It is nearly independent of detail thickness and it has a value of about 1.15.

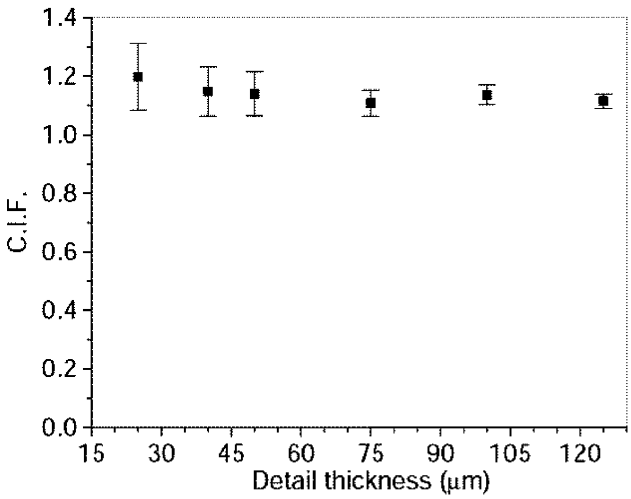

Fig. 3. CIF= $C_{\rm collimated}/C_{\rm open}$ for images of aluminum details of different thickness acquired with an irradiation field area of 361 mm^2 instead of open field. The distance between phantom and detector is 1 cm.

C. Contrast Improvement With the Distance Phantom-Detector

An improvement of the contrast can be also achieved by increasing the distance between the phantom and the detector. This method, known as "air gap method," can be explained by the fact that the contribution of the scattered photons is geometrically reduced when the phantom-detector distance is increased.

Looking at Fig. 1, we can see that the relative difference between the number of counts/pixel of the image taken with an open field $(N_{\rm open})$ and the number of counts/pixel of the image taken with a radiation field of area x (N_x) decrease of about 88%, if the distance phantom-detector varies from 1 (crosses) to 7 cm (squares) for an irradiation field area of about 5600 mm^2, but decrease of an amount only 6% if the irradiation field area is 361 mm^2.

The contrast improvement with distance is important, especially for wide irradiation field areas. In fact, in the case of an irradiation field area of 361 mm^2 the contrast poorly depends on the phantom-to-detector distance. In fact, Fig. 4 shows, for a chosen detail thickness, that for distances ranging from 1 to 4 cm, the contrast gain is about 5% and it remains constant for greater distances.

Fig. 5 shows the calculated contrast of aluminum details of different thickness for an open field acquisition (square) and for an irradiation field area of 361 mm^2 (cross) with a distance between the phantom and the detector of 7 cm. Comparing this

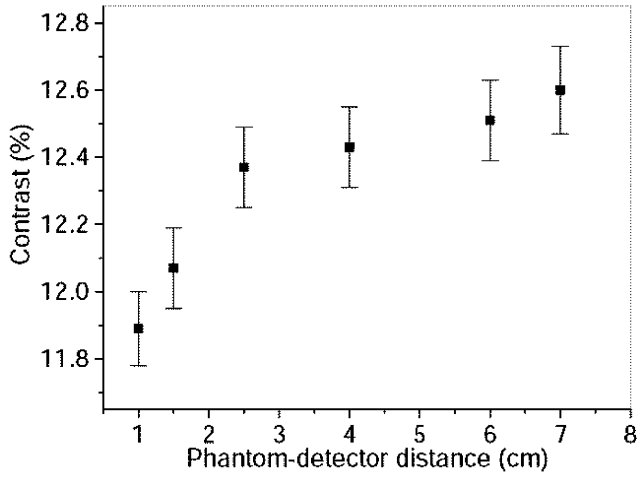

Fig. 4. Experimental contrast of a 125-μm-thick aluminum detail versus phantom-detector distance for an irradiation field area of 361 mm^2.

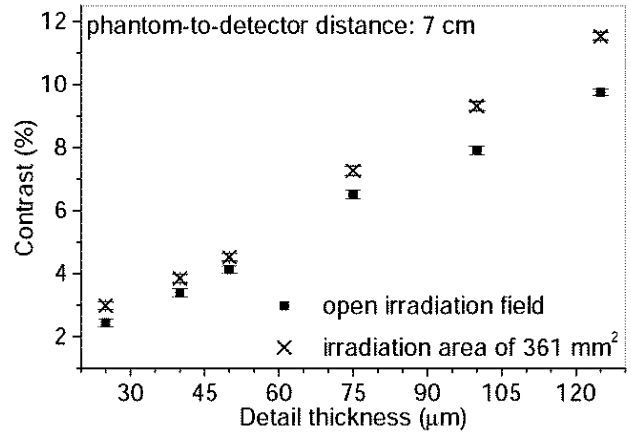

Fig. 5. Calculated contrast of aluminum details of different thickness for an open field acquisition (squares) and for an acquisition with an irradiation field area of 361 mm^2 (crosses). The error bars represent the statistic error. The distance between the phantom and the detector is 7 cm.

data with the one of Fig. 2, we can see an improvement of the contrast values.

D. Imaging Performance

The reduction of the scatter fraction leads to an improvement in imaging quality. In order to evaluate this effect, we acquired some images for aluminum details of different thickness. All the images were acquired using an energy threshold discriminator fixed at the value of about 9 keV. To take into account the systematic noise due to the different response of the 4096 pixels, each image is corrected with a gain matrix evaluated using a ^{109}Cd source (energy $\sim$ 22 keV).

To measure the efficiency correction map for the detector, data are acquired with the 64 $\times$ 64 pixel detector at a source-to-detector distance of about 10 cm so that a uniform irradiation from the source can be expected. The differences in counts between pixels will be due to the variations in intrinsic

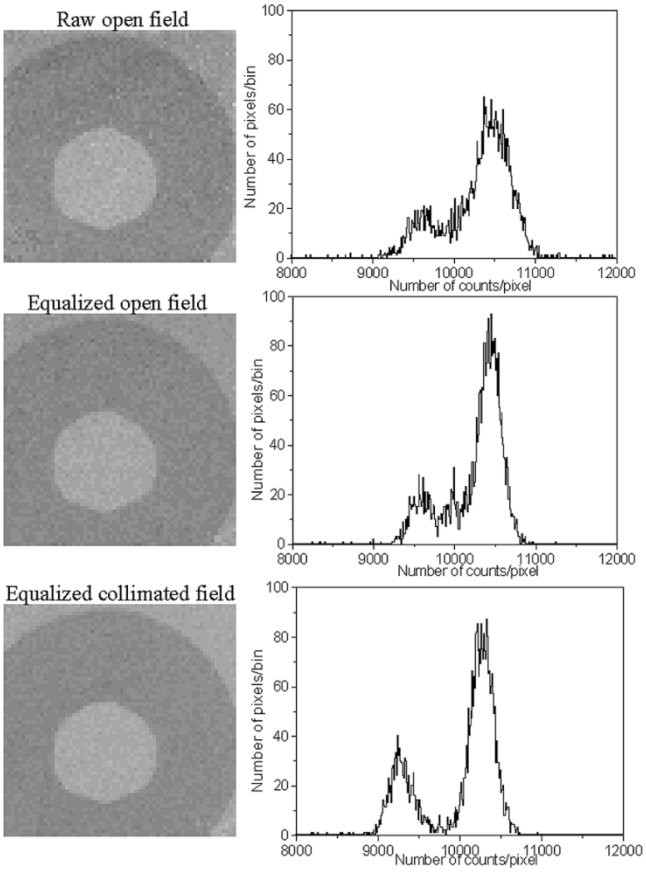

Fig. 6. Images of an aluminum detail of thickness 125 μm. The first one is the raw data image acquired with an open irradiation field, the second is the equalized image acquired with an open irradiation field, the third is the equalized image acquired with an irradiation area of 361 mm^2. The equalization of images is obtained dividing the raw data image by the gain matrix calculated with the ^{109}Cd source. Each histogram represents the counts/pixel distribution for the corresponding whole image. The distance phantom-detector is 1 cm.

efficiency among the pixels. If we divide the number of counts of every pixel by the mean number of counts/pixel registered on the whole matrix, we obtain a gain matrix.

The same thing would have been done with the mammographic tube; the choice of the ^{109}Cd source is related to the fact that small variations in the threshold value of the discriminator are negligible when the incoming photons have an energy considerably bigger than the threshold (as in the case of ^{109}Cd source, $E_\gamma \sim 22$ keV), but become relevant with the low energy component of the mammographic spectrum.

Fig. 6 shows the comparison between the raw data image and the equalized image of a 125 μm thick aluminum detail acquired using the mammographic tube (75 mAs, 28 kVp, focus-to-phantom distance of 63 cm). The equalized image is obtained by dividing the raw data image by the gain matrix evaluated with ^{109}Cd source. Each histogram shows the counts/pixel distribution for the corresponding whole image; the external peaks are the count distributions in the aluminum region (left) and in the wax region (right). After equalization, the mean is the same, however the peaks are narrower.

The third image in Fig. 6 shows the same 125 μm thick aluminum detail acquired with an irradiation field area of 361 mm^2 after the equalization; we used higher exposures (100 mAs) in

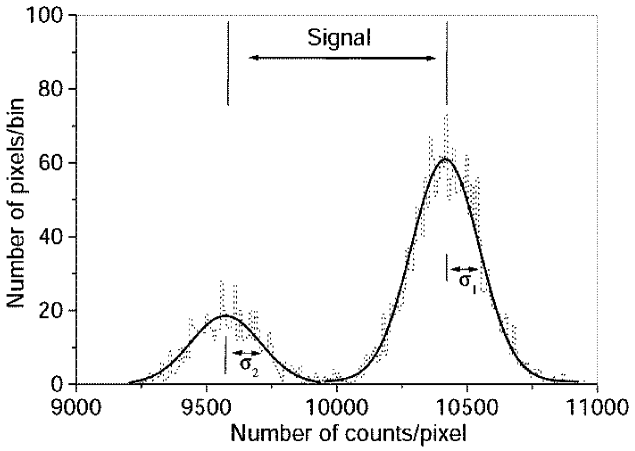

Fig. 7. Distribution of counts/pixel in the region of the wax (right peak) and aluminum (left). Each peaks is fitted with a Gaussian curve.

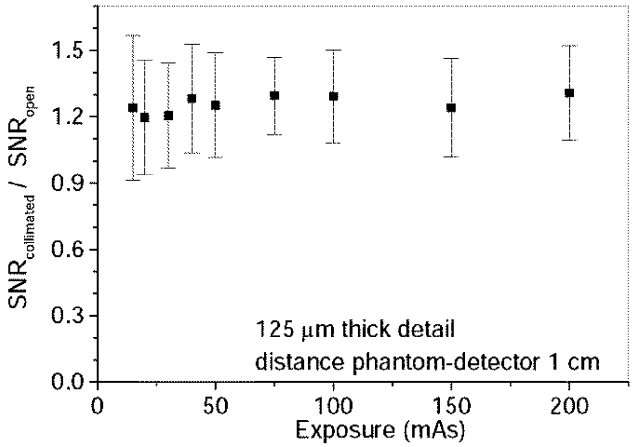

Fig. 9. SNR calculated for the collimated field over SNR calculated for the open field. The distance phantom-detector is 1 cm.

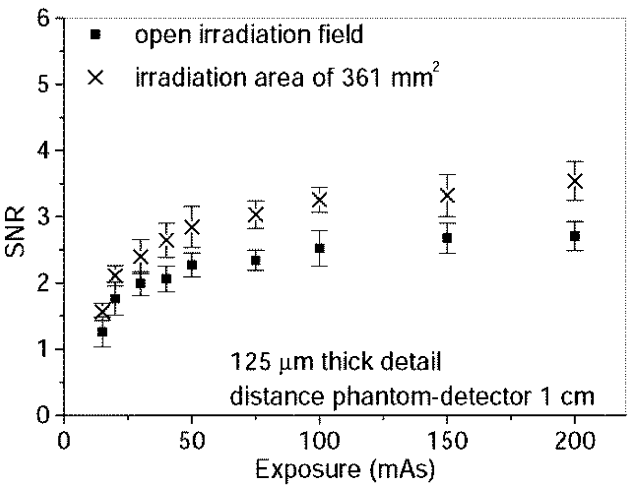

Fig. 8. SNR of the images of the 125 μm aluminum detail calculated for an open irradiation field (crosses) and for an irradiation field area of 361 mm^2. The distance phantom detector is 1 cm.

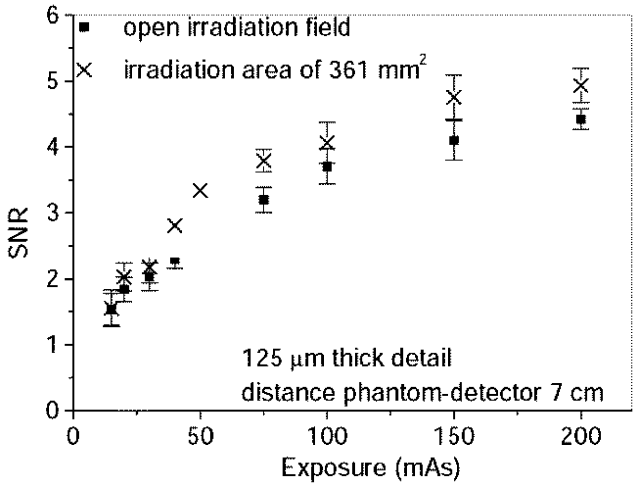

Fig. 10. SNR of the images of the 125-μm aluminum detail calculated for an open irradiation field (crosses) and for an irradiation field area of 361 mm^2. The distance phantom detector is of 7 cm.

order to have comparable statistic in all three images. Comparing the count distribution in the two equalized images we can see that, for the collimated field, the peaks are narrower and better resolved.

Signal-to-noise ratio (SNR) is a measure of improved describes imaging capabilities with collimation. In order to evaluate it, we acquired images of the 125-μm thick aluminum detail for different values of the anode current in the mammographic tube (which is proportional to exposure).

The distribution of counts/pixel obtained for the 125 μm thick aluminum detail in a region of interest which comprises only the aluminum detail (left peak) and the wax circle (right peak) is presented in Fig. 7. We used an exposure of 75 mAs and an open irradiation field. The two peaks are fitted with a Gaussian curve with mean value N_i and standard deviation σ_i ($i = 1$ means wax; $i = 2$ means aluminum).

We define SNR as

$$SNR = \frac{N_1 - N_2}{\sqrt{\sigma_1^2 + \sigma_2^2}}. \quad (4)$$

Fig. 8 shows the SNR of the images of the 125 μm aluminum detail calculated for an open irradiation field (crosses) and an irradiation field of area 361 mm^2 (circles). The distance phantom-detector is 1 cm.

The SNR increases of about 80% going from an exposure of 15 mAs to an exposure of 50 mAs and it remains constant up to 200 mAs. Moreover, the SNR calculated for the collimated field is about 25% higher than the SNR calculated for the open field.

The SNR calculated for the collimated field over the SNR calculated for the open field is reported in Fig. 9. The ratio does not depend on the exposure, which suggests that the improving of the SNR is a consequence of the collimation and it is not conditioned by any statistical effect. We made the same SNR measurements for a phantom-to-detector distance of 7 cm (Fig. 10). For exposures bigger than 50 mAs, the SNR value calculated at 7 cm is larger than that calculated at 1 cm and (for both open field and collimated field) for exposure lower than 50 mAs, which is the range commonly used in mammography, the difference become negligible.

The improvement in contrast and SNR with collimation is qualitatively shown in the images of the aluminum details of

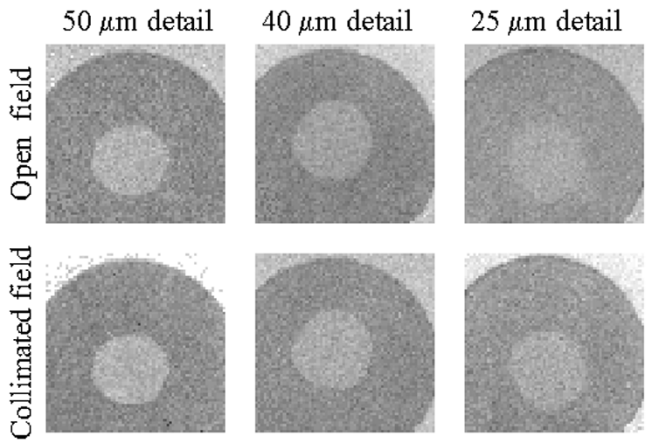

Fig. 11. Images of aluminum details of different thickness for a phantom-to-detector distance of 1 cm. In the first row, the images are acquired with an open irradiation field. In the second row, the images are acquired with an irradiation field area of 361 mm^2. All the images are equalized.

different thickness acquired at a phantom detector distance of 1 cm (Fig. 11). The dimension of each image is 1.18 cm^2; all of them have been equalized with the procedure described previously and they have been obtained with 100 mAs and 28 kVp. In the first row, the images are acquired with an open irradiation field.In the second row, the images have been acquired with an irradiation field area of 361 mm^2.

IV. Conclusion

In this work, we have evaluated how an irradiation area comparable to the area of the detector acts positively on the quality of the radiological image. In particular, using a single photon counting device based on a silicon pixel detector with an active area of 1.2 cm^2, we have studied how the contrast and the SNR in images of aluminum detail of different thickness depend on the irradiation areas and on the phantom-to-detector distance.

We have obtained a contrast improvement of about 15% going from an open field irradiation area to an irradiation area of 361 mm^2; in this case, the SNR increases about 25%. On the other hand, for a collimated field, the contrast seems depend on the poorly phantom-to-detector distance. In addition, for exposures ranging from 15 to 50 mAs, the variation of SNR with distance is negligible.

References

[1] M. Säbel and H. Aichinger, "Recent development in breast imaging," *Phys. Med. Biol.*, vol. 41, pp. 315–368, 1996.

[2] M. Sanborg and G. A. Carlsson, "Influence of X-ray energy spectrum, contrasting detail and detector on the signal-to-noise-ratio (SNR), and detective quantum efficiency (DQE) in projection radiography," *Phys. Med. Biol.*, vol. 37, pp. 1245–1263, 1992.

[3] H.-P. Chan and K. Doi, "Physical characteristic of scattered radiation in diagnostic radiology: Monte Carlo simulation studies," *Med. Phys.*, vol. 12, no. 2, pp. 152–155, 1985.

[4] M. Giannelli, "Simulazione di rivelatori a mosaico a pixel di GaAs per imaging medico," M.S. thesis, Univ. of Pisa, Pisa, Italy, 1998.

[5] M. A. Ciocci, "Scattering suppression in digital radiography," in *Proc. of 8th Pisa Meeting on Advanced Detectors 2000*. La Biodola, Isola d'Elba: Italy Nucl. Instr. Meth., May 21–27, 2001, vol. A461.

[6] M. G. Bisogni, S. Bottari, M. A. Ciocci, M. E. Fantacci, P. Maestro, N. Malakhov, P. S. Marrocchesi, M. Novelli, M. Quattrocchi, F. Pilo, V. Rosso, N. Turini, and S. Zucca, "Experimental test of a new technique of background suppression in digital mammography," in *Proc. 9th Vienna Conf. Instrumentation*, Vienna, Austria, Feb. 19–23, 2001.

[7] M. G. Bisogni, M. Campbell, M. Conti, P. Delogu, M. E. Fantacci, E. H. M. Heijne, P. Maestro, G. Magistrati, V. M. Marzulli, G. Meddeler, B. Mikulec, E. Pernigotti, V. Rosso, C. Schwarz, W. Snoeys, and S. Stumbo, "Performance of a 4096 pixel photon counting chip," in *SPIE's 43rd Annu. Meeting*, vol. 3445, San Diego, CA, July 19–24, 1998, pp. 298–304.

[8] S. R. Amendolia, M. G. Bisogni, U. Bottigli, M. A. Ciocci, P. Delogu, G. Dipasquale, M. E. Fantacci, M. Giannelli, P. Maestro, V. M. Marzulli, E. Pernigotti, V. Rosso, A. Stefanini, and S. Stumbo, "Low contrast imaging with a GaAs pixel digital detector," in *Proc. Conf. Records of Nuclear Science Symp. and Medical Imaging Conf.*, Seattle, WA, Oct. 24–30, 1999.

[9] ——, "Low contrast imaging with a GaAs pixel digital detector," *IEEE Trans. Nucl. Sci.*, vol. 47, pp. 1478–1482, Apr. 2000.